Thermoelectricity

DOI: 10.1002/anie.200803934

Large Enhancements in the Thermoelectric Power Factor of Bulk PbTe at High Temperature by Synergistic Nanostructuring**

*Joseph R. Sootsman, Huijun Kong, Ctirad Uher, Jonathan James D'Angelo, Chun-I Wu, Timothy P. Hogan, Thierry Caillat, and Mercouri G. Kanatzidis**

Thermoelectric heat-to-electrical-energy converters will play a role in energy management if efficient, stable, and inexpensive materials can be developed. Research to increase the figure of merit ZT is focused on a variety of novel thermoelectric materials and approaches.[1–9] Significant advances have come in recent years from the development of nanostructured semiconductors both in thin-film[10] and bulk form.[11–14] In the thin films, values $ZT > 3$ have been claimed for PbTe/PbSe superlattice structures,[15] while values of 1.5–1.7 at 700 K have been reported for $AgPb_{18}SbTe_{20,}$[12] $NaPb_{20}SbTe_{22}$,[16] PbTe–PbS,[17] and Tl–PbTe.[18] This progress promises to impact several energy-conversion applications. The advancements have primarily come from sizeable reductions in thermal conductivity, which is largely the result of the scattering of mid- and long-wavelength phonons at the interfaces of the nanoscale inclusions at high temperature.[18,19]

Although further increases in ZT can be anticipated by additional reduction of the thermal conductivity, a lower limit is expected to be reached. Thus, dramatic enhancements in ZT can only come from spectacular increases in the power factor ($S^2\sigma$). This problem is harder to tackle, since standard charge-transport theory does not offer specific guidance on how to dramatically increase the power factor. Its solution will require breakthroughs in the understanding and control of charge-transport mechanisms in complex materials. An important factor affecting charge transport (e.g. mobility $\mu = e\tau/m$, where m is the carrier effective mass) and thus power factor in solids is the relaxation time τ, which has an energy dependence [Eq. (1), where E is the energy and r is a

$$\tau = \tau_o E^{r-1/2} \quad (1)$$

scattering parameter].[20] This relationship implies that the energy dependence of τ impacts the mobility, electrical conductivity ($\sigma = Ne\mu$, N = carrier concentration), and thermopower in semiconductors, especially for large values of r owing to their dependence on the relaxation time. In PbTe it is not possible to cause significant changes in the scattering mechanism by making solid solutions or through carrier doping.[21] A more fundamental question is whether the relative contributions of known scattering mechanisms, or even the actual mechanisms themselves in PbTe, can be altered through nanostructuring. For example, can features buried on the nanoscale fundamentally change the electronic structure and therefore charge transport?

We report herein a new way to achieve dramatic changes in the carrier transport in PbTe, which leads to large increases in the thermoelectric power factor ($S^2\sigma$) at high temperatures. We observe the enhancements only when PbTe is co-nanostructured with two different phases. We show that when lead and antimony are present simultaneously as nanodots throughout the matrix of PbTe, the conductivity behavior becomes novel. We observe unprecedented temperature dependence that is a complicated function of the Pb/Sb ratio. The most important consequence is that for certain carrier concentrations the power factor changes its typical temperature dependence, and instead of falling with temperature it actually rises, thus giving a large enhancement at high temperatures (above 600 K). To our knowledge, these observations underscore a novel combination of physical mechanisms by which carrier propagation can occur in PbTe.

Previous reports have shown that the Seebeck coefficient can be increased in PbTe by the inclusion of excess Pb precipitated on the nanoscale; this effect was attributed to an increase in the scattering parameter r.[20] However, the power factor decreased in this case because of lower electron mobilities. In the present study, we prepared PbTe with Pb and Sb nanoinclusions through the matrix encapsulation technique.[22] This method produces a material with 2–10 nm nanodots of Sb and Pb simultaneously embedded and dispersed in the PbTe matrix. At concentrations over 0.5 atom %, micrometer-sized regions consisting of a Pb/Sb eutectic also precipitate at the PbTe grain boundaries. Pb and Sb do not form a compound[23] but rather have a eutectic-type

[*] J. R. Sootsman, Prof. M. G. Kanatzidis
Department of Chemistry, Northwestern University
2145 Sheridan Rd. Evanston, IL 60208 (USA)
Fax: (+1) 847-491-5937
E-mail: m-kanatzidis@northwestern.edu
H. Kong, Prof. C. Uher
Department of Physics, University of Michigan
Ann Arbor, MI 48109 (USA)
J. J. D'Angelo, Dr. C.-I. Wu, Prof. T. P. Hogan
Department of Electrical and Computer Engineering
Michigan State University
East Lansing, MI 48824 (USA)
Dr. T. Caillat
Jet Propulsion Laboratory, California Institute of Technology
Pasadena, CA 91109 (USA)

[**] The authors would like to thank the Office of Naval Research (MURI program) for funding. Portions of the scanning and transmission electron microscopy work was performed in the (EPIC) (NIFTI) (Keck-II) facility of NUANCE Center at Northwestern University. NUANCE Center is supported by NSF-NSEC, NSF-MRSEC, Keck Foundation, the State of Illinois, and Northwestern University.

Supporting information for this article is available on the WWW under http://dx.doi.org/10.1002/anie.200803934.

phase relationship, where they are soluble in each other in the liquid but are insoluble in the solid state. Pb and Sb also have low solubility in PbTe,[24,25] giving these elements the ability to form nanodots upon fast cooling.[22] The concentration of Pb and Sb in PbTe was varied from 0.5 to 3%. Typical powder X-ray diffraction patterns for various PbTe samples with Pb and Sb nanodots are shown in Figure 1a.

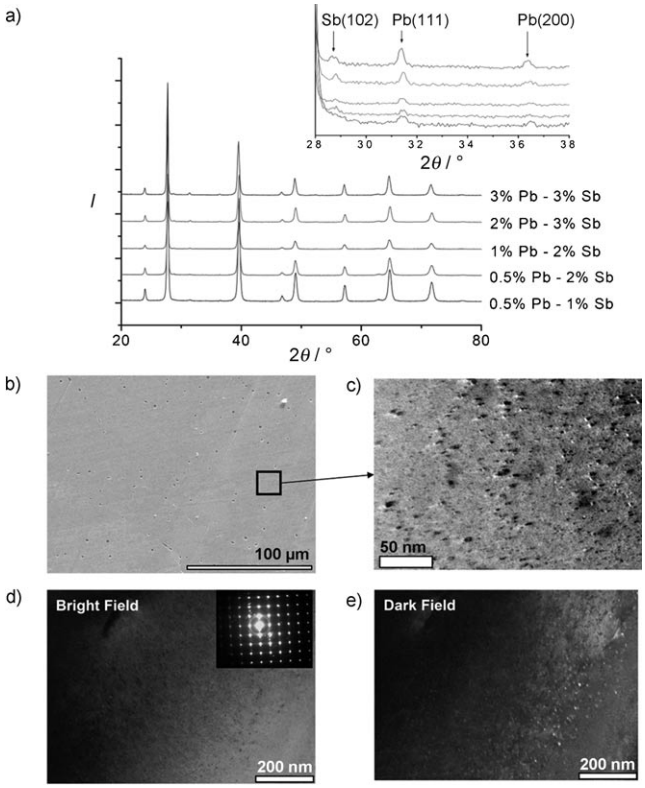

Figure 1. a) Powder X-ray diffraction patterns for several PbTe–Pb–Sb materials ($Cu_{K\alpha}$ radiation). Inset shows the presence of the Sb(102), Pb(111), and Pb(200) reflections and their scaling with Pb and Sb concentration. b) SEM image of the grains of co-nanostructured PbTe. c) TEM image of several nanocrystals embedded in the PbTe matrix. d) Bright-field TEM image showing dispersed nanoscale precipitates. Inset: electron diffraction pattern revealing the NaCl structure of the matrix and the additional weak reflections from the Pb and Sb phases. e) Dark-field TEM image generated from the weak reflections (not belonging to PbTe) in the electron diffraction pattern. High-resolution transmission electron microscopy (TEM) was carried out using a JEOL-2200FS field emission gun microscope.

Scanning and transmission electron microscopy reveal the micro- and nanostructure of the composites, showing that a large proportion of Pb and Sb precipitate on the nanoscale, with sizes varying from 2–20 nm, and the rest precipitates on the microscale. A representative scanning electron micrograph for the PbTe–Pb(0.5%)–Sb(2%) sample is shown in Figure 1b. Backscattered electron images, which can determine compositional differences in microstructure, show two distinct regions within the samples: the major PbTe phase and the minor Pb and Sb phases. When the concentrations are greater than 2–3% excess, Pb and Sb precipitate as a eutectic at the grain boundaries of PbTe, whereas below 2% only isolated island regions were observed. Overall, at low magnification the elemental composition according to energy dispersive spectroscopy (EDS) agreed with the nominal composition. The major PbTe grains contain embedded and dispersed nanodots of Sb and Pb, which are revealed by transmission electron microscopy (TEM).

TEM shows that within the PbTe domains there is good dispersion of spheroidal particles throughout the sample on the 3–8 nm scale (Figure 1c–e). The composition of the individual particles was difficult to determine, but selected area electron diffraction (SAED) indicated, in addition to PbTe reflections, diffraction spots arising from the Pb and Sb nanocrystals. (Figure 1d inset). These additional reflections were used to generate the dark-field image shown in Figure 1e. The presence of these nanocrystals is believed to be responsible for the profound effects on the electrical transport in this system that result in large increases in power factor.

Electrical conductivity data from PbTe–Pb–Sb samples taken between 300 and 675 K reveal a very different temperature dependence compared to that of PbTe itself or PbTe nanostructured either with Sb or Pb nanodots (Figure 2a). This difference is better illustrated by considering the temperature dependence of the conductivity, which can be done by fitting the data to a power law $\sigma \approx \sigma_o T^{\alpha}$. The power exponent α is related to the r parameter of Equation (1) and is tightly coupled to electron phonon scattering. In the degenerately doped case, α is not influenced by changes such as solid solution alloying and doping. For a constant carrier concentration, the α value derives from the temperature dependence of the mobility ($\mu \approx T^{\alpha}$) and is a function of the scattering time.[21]

For pure PbTe, the canonical power law dependence of the mobility has exponent α close to -2.5 ± 0.3.[21,26] This property is intrinsic to the material[21,26] and does not significantly change in nanostructured samples of PbTe–Pb and PbTe–Sb (Figure S1 in the Supporting Information). In the co-nanostructured samples, however, the α value appears to be a strong function of the Pb/Sb ratio. The exponent α varied from -2.1 to $+0.68$ as the ratio increased from Sb/Pb ≈ 0.25 (Sb-rich) to approximately 1 (Table 1). The total concentration also tunes the temperature dependence: A large concentration of Pb + Sb shows a greater tendency toward lower power α values, remarkably even achieving a sign reversal at PbTe–Pb(3%)–Sb(3%). The implication of an exponent that is lower than for PbTe (i.e. $\alpha < -2.5$) is that the electrical conductivity at high temperatures will be much larger than that of PbTe itself, even if the room-temperature values were comparable. Thus, the significant deviation in this power law behavior when both Pb and Sb nanoparticles are present would imply a marked change in how carrier scattering occurs. Because the Seebeck coefficient of these samples is in fact "normal" and increases linearly with temperature, this causes large increases in the power factor at high temperature relative to conventional PbTe of the same carrier concentration (see below).

For co-nanostructured samples with low Pb/Sb ratio (less than 0.5), electrical conductivities of greater than 2000 $S\,cm^{-1}$ were observed at room temperature. The power law fit of α

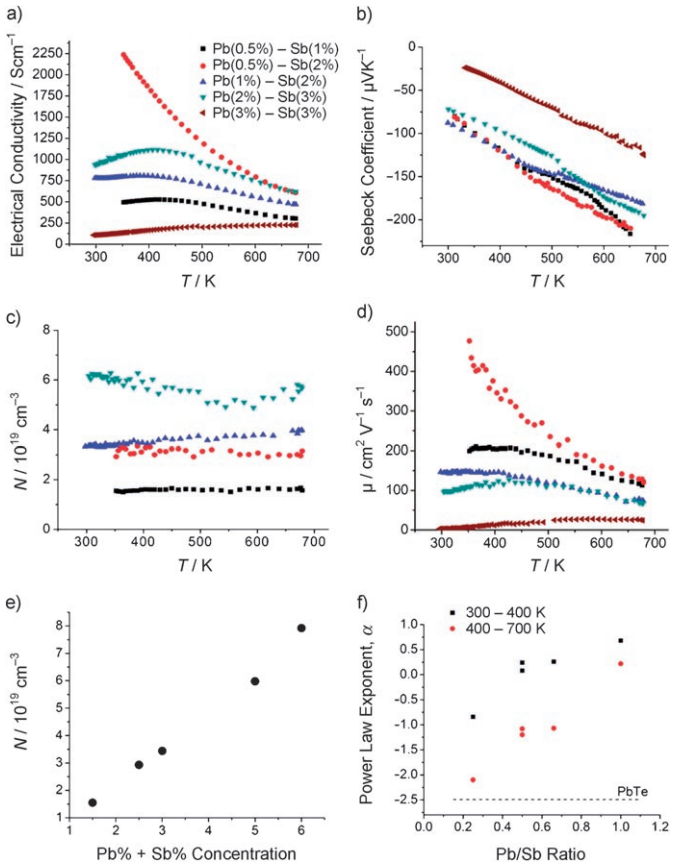

Figure 2. a) Electrical conductivity, b) Seebeck coefficient, c) carrier concentration, and d) mobility as a function of temperature for selected co-nanostructured PbTe–Pb–Sb materials. e) Dependence of carrier concentration on the total (Pb + Sb) concentration in PbTe. f) Power law fits (exponent α) of the mobility for given Pb/Sb ratio in the temperature ranges 300–400 K and 400–700 K. The dotted horizontal line is the canonical power exponent for pure PbTe. Electrical conductivity, Seebeck coefficient, and Hall coefficient measurements were performed as described elsewhere.[28]

Table 1: Exponent values (α) extracted from the temperature-dependent mobility data of co-nanostructured samples of PbTe–Pb–Sb as a function of Pb/Sb ratio and (Pb + Sb) concentration. The mobility was fit according to $\mu = \mu_0 T^{\alpha}$ for temperatures between 300–400 K and 400–700 K showing the strong dependence the fit has on the Pb/Sb ratio.

Pb/Sb	Pb + Sb [%]	α (300–400 K)	α (400–700 K)
–	0[a,b]	−2.50	−2.50
0.25	2.5	−0.84	−2.10
0.5	1.5	0.24	−1.2
0.5	3	0.08	−1.08
0.66	5	0.26	−1.07
1	6	0.68	0.22

[a] Pure PbTe (degenerate doping n-type). [b] In samples of PbTe nanostructured only with Sb or Pb, α is ca. −1.8–2.2 (regardless of concentration).

was −1.8–2.2 for samples with this ratio, which is lower than the −2.5 observed for doped PbTe. As the ratio of Pb/Sb is increased, the electrical conductivity is reduced to between 500–2000 S cm^{-1}, and the power exponent α is in the range of approximately 1 to −0.5, depending on the ratio. When the concentration of Pb was 1 % and of Sb was 2 %, the electrical conductivity remained constant from 300–450 K (ca. 700 S cm^{-1}) and fell only very slowly from 450–675 K (Figure 2a). Remarkably, when the concentration of Pb was 2 % and of Sb was 3 %, the high room-temperature electrical conductivity of approximately 950 S cm^{-1} actually increased with increasing temperature, reaching about 1100 S cm^{-1} at 450 K before it started to fall, albeit very slowly, to approximately 600 S cm^{-1} at 700 K (Figure 2a). The rising electrical conductivity with increasing temperature (above 300 K) in highly doped PbTe materials is unique and has only been observed through a hopping mechanism previously reported for indium-doped PbTe,[27] although the mobility in the previous example was significantly degraded compared to the present materials. The changes in temperature dependence of the conductivity imply a dramatic change in how electrons scatter at these temperatures.

The anomalous temperature dependence of the conductivity in the Pb/Sb co-nanostructured PbTe samples cannot be attributed to a changing carrier concentration. As seen in Figure 2b, the temperature dependence of the Seebeck coefficient in all samples is linear. Room-temperature values of the Seebeck coefficient range from −30 to −80 μV K^{-1} and increase in magnitude to between −160 and −200 μV K^{-1} at 675 K. The values of the Seebeck coefficient indicate n-type behavior. The temperature dependence was reproducible in all of the samples to within ±10 % in the absolute magnitude of the values measured. The linearity in the Seebeck coefficient data is normal and suggests that the carrier concentration is constant. This conclusion is also supported by the Hall-effect measurements discussed below.

The Hall coefficients measured between 300 and 700 K were negative, indicating n-type conduction, in agreement with the Seebeck measurements. The carrier concentration was essentially constant (Figure 2c) over the measured range, and so the Hall mobility follows the same trends as the electrical conductivity (Figure 2d). The electron mobility μ was calculated from the electrical conductivity, assuming one carrier type in a single-band approximation ($\sigma = Ne\mu$). The carrier concentration N, obtained from the Hall coefficient, scales with the levels of dopants Sb and Pb (Figure 2e). The exponent α, however, and the dependence of the mobility appear to be a rather complex function of the Pb/Sb ratio as well as Pb and Sb concentration (Figure 2f). At 350 K in PbTe–Pb(0.5 %)–Sb(2 %), the carrier mobility remained high (ca. 478 cm^2 V^{-1} s^{-1}); however, when the concentration of Sb was reduced to 1 % with the same concentration of Pb(0.5 %), the mobility decreased, though to a still considerable value of approximately 200 cm^2 V^{-1} s^{-1}. The sample PbTe–Pb(2 %)–Sb(3 %) actually showed an increase in mobility with increasing temperatures (i.e. thermally activated behavior), reaching a maximum before it began to fall at higher temperatures.

Although ionized impurity scattering can result in rising mobilities with increasing temperature, this mechanism is known to be important only at low temperatures (i.e. well below 300 K). The phenomena described herein occur several hundred degrees above room temperature, which excludes conventional ionized impurity scattering as the cause. The

transport results show that at higher temperature a higher-than-expected mobility (i.e. less scattering) is present in the PbTe–Pb–Sb samples.

The slower rate of decrease in mobility in the co-nanostructured PbTe systems gives rise to a much higher power factor at higher temperatures than otherwise would be expected for the same carrier concentration in PbTe. This changes the typical trend of a falling power factor in conventional PbTe ($N = 3 \times 10^{19}$ cm^{-3}) samples to a rising power factor with increasing temperature (Figure 3a). The significant enhancement in the co-nanostructured PbTe–Pb–Sb compared to PbTe itself, particularly at high temperatures, is more clearly shown when power factors are compared for corresponding samples of the same carrier concentration. Figure 3a,b compares two sets of samples with $N \approx 3 \times 10^{19}$ cm^{-3} and 6×10^{19} cm^{-3}, respectively, showing 71 and 43% increase at approximately 700 K. This increase arises from the modified exponent α in the mobility that results in excess conductivity at 700 K, discussed above and compared in Figure S2 in the Supporting Information. Smaller enhancements were observed in other carrier concentrations.

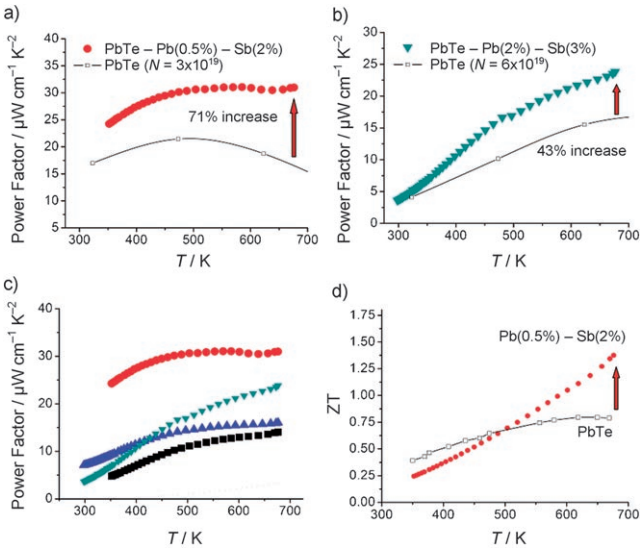

Figure 3. a) Comparison of the power factors of co-nanostructured PbTe and conventional PbTe[21] for the carrier concentration $N \approx 3 \times 10^{19}$ cm^{-3}. b) Comparison of the power factors of co-nanostructured PbTe and conventional PbTe for the carrier concentration $N \approx 6 \times 10^{19}$ cm^{-3}. c) Temperature dependence of the power factors of selected co-nanostructured PbTe samples. The sample color code is the same as Figure 2a. d) Comparison of ZT between co-nanostructured PbTe–Pb(0.5%)–Sb(2%) and conventional optimized PbTe as a function of temperature.

Because nanoparticles also reduce the lattice thermal conductivity, considerable ZT enhancements can be achieved in selected co-nanostructured PbTe–Pb–Sb materials compared to other PbTe samples of similar carrier concentrations. For example, in PbTe–Pb(0.5%)–Sb(2%), the lattice thermal conductivity at 650–700 K is 0.6 W mK^{-1}, and coupled with an enhanced power factor, a ZT of 1.4 was attained at 650–700 K (Figure 3d). Because of the high carrier concentrations in these samples (degenerate doping), peaking of the Seebeck coefficient is not expected until much high temperatures (ca. 850–900 K). If true, we may anticipate ZT values of approximately 1.8 at these temperatures.

We have shown that the temperature dependence of the mobility in the co-nanostructured PbTe materials departs significantly from the standard transport model for PbTe. This new transport model achieves a larger electrical conductivity at high temperatures without loss of thermopower, thereby producing large power factor enhancements. We observe the new behavior only when nanodots of Pb and Sb are simultaneously present. Simple nanostructuring with either Pb or Sb nanodots alone does not give rise to the phenomena described herein. Because this behavior cannot be directly traced to the system's individual components, but rather to how those components interact, it is difficult at this stage to account for its cause. This is therefore emergent behavior and gives the system radical novelty (features not previously observed in thermoelectric materials). Regardless of its origin, semiconductor co-nanostructuring is a concept that should be applicable to other thermoelectric materials and can serve as a foundation for identifying design principles to achieve very large enhancements in power factor and ZT at high temperatures.

Experimental Section

Stock PbTe was prepared from high-purity Pb and Te (Plasmaterials, 99.999%) in several 100–200 g batches in evacuated quartz ampoules at 1273 K. The addition of excess Pb and Sb in the appropriate molar ratios was then carried out on a 10 g scale using Pb and Sb metals (Tellurex, 99.999%). The samples were heated to the melt, held at the isotherm for 10–15 h, then rapidly cooled from 1273 K in a water bath. Samples were then cut and polished for thermal and electrical transport, microscopic investigation, and powder X-ray diffraction. Qualitative compositional analysis was performed using a JEOL JSM-35C scanning electron microscope (SEM) equipped with a Tracor Northern EDS detector.

Received: August 8, 2008
Published online: October 7, 2008

Keywords: composite materials · nanostructures · semiconductors · thermoelectric materials

[1] J. J. Urban, D. V. Talapin, E. V. Shevchenko, C. R. Kagan, C. B. Murray, *Nat. Mater.* **2007**, *6*, 115.
[2] H. Ohta, S. Kim, Y. Mune, T. Mizoguchi, K. Nomura, S. Ohta, T. Nomura, Y. Nakanishi, Y. Ikuhara, M. Hirano, H. Hosono, K. Koumoto, *Nat. Mater.* **2007**, *6*, 129.
[3] P. Reddy, S. Y. Jang, R. A. Segalman, A. Majumdar, *Science* **2007**, *315*, 1568.
[4] Y. Y. Wang, N. S. Rogado, R. J. Cava, N. P. Ong, *Nature* **2003**, *423*, 425.
[5] T. C. Harman, P. J. Taylor, M. P. Walsh, B. E. LaForge, *Science* **2002**, *297*, 2229.
[6] R. Venkatasubramanian, E. Siivola, T. Colpitts, B. O'Quinn, *Nature* **2001**, *413*, 597.
[7] D. M. Rowe, *CRC Handbook of Thermoelectrics*, CRC, Boca Raton, FL, **1995**.
[8] A. I. Hochbaum, R. K. Chen, R. D. Delgado, W. J. Liang, E. C. Garnett, M. Najarian, A. Majumdar, P. D. Yang, *Nature* **2008**, *451*, 163.

[9] A. I. Boukai, Y. Bunimovich, J. Tahir-Kheli, J. K. Yu, W. A. Goddard, J. R. Heath, *Nature* **2008**, *451*, 168.
[10] H. Bottner, G. Chen, R. Venkatasubramanian, *MRS Bull.* **2006**, *31*, 211.
[11] J. Androulakis, K. F. Hsu, R. Pcionek, H. Kong, C. Uher, J. J. Dangelo, A. Downey, T. Hogan, M. G. Kanatzidis, *Adv. Mater.* **2006**, *18*, 1170.
[12] K. F. Hsu, S. Loo, F. Guo, W. Chen, J. S. Dyck, C. Uher, T. Hogan, E. K. Polychroniadis, M. G. Kanatzidis, *Science* **2004**, *303*, 818.
[13] P. F. P. Poudeu, J. D'Angelo, H. J. Kong, A. Downey, J. L. Short, R. Pcionek, T. P. Hogan, C. Uher, M. G. Kanatzidis, *J. Am. Chem. Soc.* **2006**, *128*, 14347.
[14] H. Wang, J. F. Li, C. W. Nan, M. Zhou, W. S. Liu, B. P. Zhang, T. Kita, *Appl. Phys. Lett.* **2006**, *88*, 092104.
[15] T. C. Harman, M. P. Walsh, B. E. Laforge, G. W. Turner, *J. Electron. Mater.* **2005**, *34*, L19.
[16] P. F. R. Poudeu, J. D'Angelo, A. D. Downey, J. L. Short, T. P. Hogan, M. G. Kanatzidis, *Angew. Chem.* **2006**, *118*, 3919 – 3923; *Angew. Chem. Int. Ed.* **2006**, *45*, 3835.
[17] J. Androulakis, C. H. Lin, H. J. Kong, C. Uher, C. I. Wu, T. Hogan, B. A. Cook, T. Caillat, K. M. Paraskevopoulos, M. G. Kanatzidis, *J. Am. Chem. Soc.* **2007**, *129*, 9780.
[18] J. P. Heremans, V. Jovovic, E. S. Toberer, A. Saramat, K. Kurosaki, A. Charoenphakdee, S. Yamanaka, G. J. Snyder, *Science* **2008**, *321*, 554.
[19] W. Kim, S. L. Singer, A. Majumdar, D. Vashaee, Z. Bian, A. Shakouri, G. Zeng, J. E. Bowers, J. M. O. Zide, A. C. Gossard, *Appl. Phys. Lett.* **2006**, *88*, 242107.
[20] J. P. Heremans, C. M. Thrush, D. T. Morelli, *J. Appl. Phys.* **2005**, *98*, 063703.
[21] B. A. E. Yu, I. Ravich, I. A. Smirnov, *Semiconducting Lead Chalcogenides*, *Vol. 5*, Plenum, New York, **1970**.
[22] J. R. Sootsman, R. J. Pcionek, H. J. Kong, C. Uher, M. G. Kanatzidis, *Chem. Mater.* **2006**, *18*, 4993.
[23] S. Ashtakala, A. D. Pelton, C. W. Bale, *Binary Alloy Phase Diagrams*, *Vol. 3* (Ed. T. B. Massalski), ASM International, Materials Park, OH, **1990**, 3009.
[24] G. W. Henger, E. A. Peretti, *J. Less-Common Met.* **1965**, *8*, 124.
[25] J. C. Lin, K. C. Hsieh, R. C. Sharma, Y. A. Chang, *Binary Alloy Phase Diagrams*, *Vol. 3* (Ed. T. B. Massalski), ASM International, Materials Park, OH, **1990**, 3017.
[26] Y. I. Ravich, I. A. Smirnov, V. V. Tikhonov, *Fiz. Tekh. Poluprovodn.* **1967**, *1*, 206.
[27] Y. I. Ravich, S. A. Nemov, *Semiconductors* **2002**, *36*, 1.
[28] H. Kong, X. Shi, C. Uher, D. T. Morelli, *J. Appl. Phys.* **2007**, *102*.

